High-Efficiency Upconversion Luminescent Sensing and Bioimaging of Hg(II) by Chromophoric Ruthenium Complex-Assembled Nanophosphors

Qian Liu,[†] Juanjuan Peng,[†] Lining Sun,[‡] and Fuyou Li[†,*]

[†]Department of Chemistry, Fudan University, Shanghai 200433, People's Republic of China, and [‡]Research Center of Nano Science and Technology, Shanghai University, 99 Shandong Road, Shanghai 200444, People's Republic of China

ABSTRACT A chromophoric ruthenium complex-assembled nanophosphor (N719-UCNPs) was achieved as a highly selective water-soluble probe for upconversion luminescence sensing and bioimaging of intracellular mercury ions. The prepared nanophosphors were characterized by X-ray powder diffraction (XRD), transmission electron microscopy (TEM), energy-dispersive X-ray analysis (EDXA), Fourier transform infrared spectroscopy (FTIR), and X-ray photoelectron spectroscopy (XPS). Further application of N719-UCNPs in sensing Hg^{2+} was confirmed by optical titration experiment and upconversion luminescence live cell imaging. Using the ratiometric upconversion luminescence as a detection signal, the detection limit of Hg^{2+} for this nanoprobe in water was down to 1.95 ppb, lower than the maximum level (2 ppb) of Hg^{2+} in drinking water set by the United States EPA. Importantly, the nanoprobe N719-UCNPs has been shown to be capable of monitoring changes in the distribution of Hg^{2+} in living cells by upconversion luminescence bioimaging.

KEYWORDS: bioimaging · ratiometric · upconversion luminescence · Hg^{2+}

Mercury, as one of the most toxic heavy metals, causes serious environmental and health problems, and it exists in a variety of different forms (metallic, ionic, and as a part of organic salts and complexes).[1] Mercuric ion (Hg^{2+}), as one of the most stable inorganic forms of mercury, can be transformed into methylmercury by microbial biomethylation in aquatic sediments, which can accumulate in the human body through the food chain and cause serious damage to the central nervous system.[1] Therefore, the detection and quantification of Hg^{2+} in environmental monitoring is of the utmost importance.[2−6]

Fluorescent chemodosimeters have become a powerful tool for sensing trace amounts of Hg^{2+} owing to their simplicity, short responsive time, and high sensitivity.[7−20] To date, some of them have been successfully applied in fluorescent imaging of Hg^{2+} in biosamples.[13−20] To develop the application of Hg^{2+}-selective fluorescent chemodosimeters in biological systems, near-infrared (NIR) light instead of UV and visible light should be a more suitable stimulating source because NIR light penetrates deeper into tissues and elicits lower autofluorescence from biosamples. The reports on the Hg^{2+}-selective chemodosimeters reliant on NIR excitation are rather rare.[20] Recently, Tian *et al.* reported one case of Hg^{2+}-selective chemodosimeters with NIR-to-NIR down-conversion fluorescence as output.[20]

Alternatively, the use of upconversion luminescence (UCL) as the detection signal has become an interesting strategy for sensing and bioimaging.[21−40] UCL of rare-earth nanophosphors is a process whereby continuous-wave (CW) low-energy light is converted into higher energy visible light through multiple-photon absorption or energy transfer.[41−56] This unique UCL mechanism allows rare-earth nanophosphors to display some special advantages as photoluminescent probes in bioimaging, such as a large anti-Stokes shift of several hundred nanometers, an absence of autofluorescence from biological samples,[32] remarkable light penetration depth in tissue,[36,38] and no photobleaching.[32,33] As a result, there is increasing interest in sensing and bioimaging based on upconversion nanophosphors as luminescent labels. For example, Wolfbeis *et al.* developed a series of UCL-based chemosensors to detect NH_3, O_2, and so on.[27−29] Unfortunately, to the best of our knowledge, no Hg^{2+}-selective fluorescence probe and imaging based on UCL has been reported to date. In the present study, an upconversion nanophosphor $NaYF_4$: 20 mol % of Yb, 1.6 mol % of Er, 0.4 mol % of Tm (abbreviated as

* Address correspondence to fyli@fudan.edu.cn.

Received for review July 13, 2011 and accepted September 7, 2011.

Published online September 07, 2011
10.1021/nn202620u

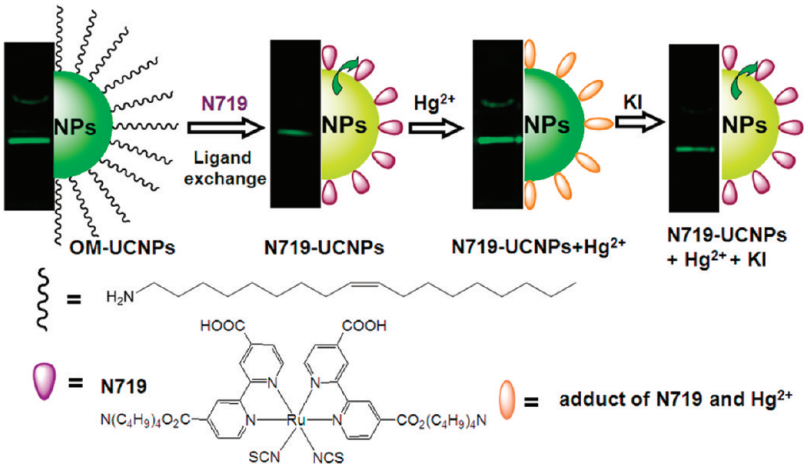

Scheme 1. Schematic illustration of synthesis of the ruthenium complex N719-modified upconversion nanophosphor $NaYF_4$: 20 mol % of Yb, 1.6 mol % of Er, 0.4 mol % of Tm (N719-UCNPs) and their upconversion luminescence (UCL) response to Hg^{2+} and further addition of KI. Change in green UCL emission is also shown in their corresponding photos (with the band-pass filter of 540 ± 5 nm). OM-UCNPs stands for oleylamine-capped UCNPs.

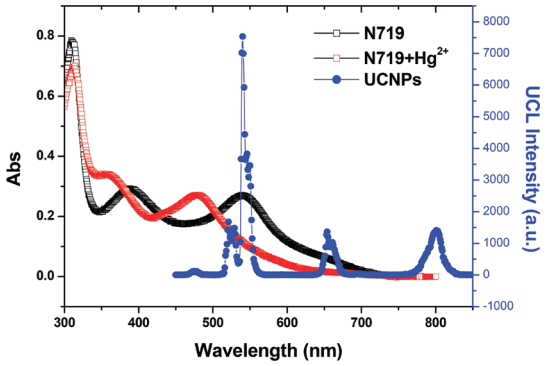

Figure 1. UV−vis spectra of the complex N719 in the absence (black) and presence of Hg^{2+} (red), and upconversion luminescence spectrum of oleylamine-coated $NaYF_4$: 20 mol % of Yb, 1.6 mol % of Er, 0.4 mol % of Tm (OM-UCNPs, blue) under excitation with 980 nm laser.

UCNPs) and the Hg^{2+}-responsive ruthenium complex N719[57−59] as an antenna species have been combined in one chromophoric upconversion nanosystem (abbreviated as N719-UCNPs; Scheme 1) to sense Hg^{2+} in aqueous solution and in living cells.

RESULTS AND DISCUSSION

Design and Principle of Hg^{2+} UCL Nanosensor. Our design strategy of Hg^{2+}-selective chromophoric upconversion nanosystem N719-UCNPs is based on Hg^{2+} modulating energy transfer degree from upconversion luminescence (UCL) emission of the nanophosphor to the absorbance of the complex N719. As shown in Figure 1, the spectral overlap between the green upconversion luminescence emission from Er^{3+}-doping UCNPs and the absorbance of the complex N719 indicates the possibility of the energy transfer process from emissive Er^{3+} to the complex N719. As reported by Palomares *et al.*,[57−59] addition of Hg^{2+} induces a significant blue shift for the absorption maximum of the complex N719, from 541 to 485 nm (Figure 1), leading to a decrease in the spectral overlap between the green upconversion luminescence emission of UCNPs and the absorption band of the complex N719, and resulting in a recovery of the upconversion luminescence emission of UCNPs at 541 nm. As a result, the nanosystem is expected to sense Hg^{2+} over other metal cations. Furthermore, to avoid the possible interference by certain factors (such as the probe concentration and environmental conditions) for upconversion luminescence intensity-based sensing, upconversion luminescence at 801 nm from Tm^{3+} was used as an internal standard and ratiometric upconversion luminescence at 541 nm to that at 801 nm (UCL_{541}/UCL_{801}) was chosen as the output signal.

Characterization of OM-UCNPs and N719-UCNPs. The ruthenium complex N719-modified upconversion nanophosphor N719-UCNPs was prepared by ligand exchange of oleylamine-coated UCNPs (abbreviated as OM-UCNPs) with the ruthenium complex N719, as shown in Scheme 1. The hexagonal OM-UCNPs were prepared by a thermal decomposition strategy with oleylamine as the surface ligand[60,61] and were characterized by X-ray powder diffraction (XRD), transmission electron microscopy (TEM), energy-dispersive X-ray analysis (EDXA), and Fourier transform infrared spectroscopy (FTIR). TEM images of OM-UCNPs and N719-UCNPs (Figure 2a,b) show polyhedron morphologies, and the average particle size is ~17 nm, which was calculated with the aid of statistical product and service solutions (SPSS). As shown in Figure S1 (Supporting Information), the XRD pattern of N719-UCNPs can be indexed to the pure hexagonal phase (JPCDS file number 16-0334) of $NaYF_4$, which was confirmed by high-resolution TEM (HRTEM) image (Figure 2c).

The assembly of the complex N719 on the surface of the UCNPs was investigated by FTIR spectrophotometry.

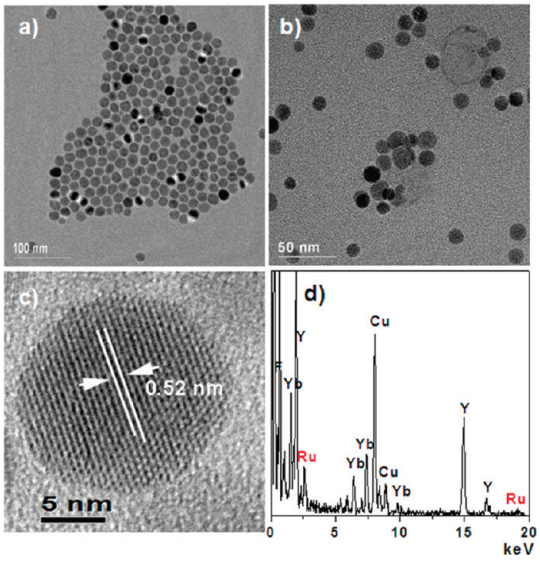

Figure 2. (a–c) TEM and HR-TEM images of OM-UCNPs (a) and N719-UCNPs (b,c). (d) EDXA of N719-UCNPs.

In the FTIR spectrum of oleylamine-coated OM-UCNPs (Figure S2), the bands at 3427 and 3354 cm^{-1} can be assigned to asymmetric and symmetric NH stretching, that at 1611 cm^{-1} can be assigned to $\delta(NH_2)$, and those at 2916 and 2852 cm^{-1} can be attributed to asymmetric and symmetric CH_2 stretching, indicating the presence of oleylamine on the surface of the OM-UCNPs. In comparison with the spectrum of oleylamine-coated OM-UCNPs, new peaks at 2104 cm^{-1} attributable to the characteristic feature of ν(NCS) and at 1365 cm^{-1} attributable to the symmetric stretch of the carboxylate group were observed in the FTIR spectrum of the ruthenium complex-modified N719-UCNPs (Figure S2), suggesting that the complex N719 had been successfully assembled on the surface of the N719-UCNPs by ligand exchange.

Moreover, the presence of the complex N719 on the surface of the as-prepared N719-UCNPs was also confirmed by X-ray photoelectron spectroscopy (XPS) and EDXA. As shown in Figure 3, the XPS patterns of ruthenium (Ru) and sulfur (S) were observed only for N719-UCNPs and not for oleylamine-coated OM-UCNPs. Similarly, the EDXA patterns showed the appearance of Ru as a new element in the N719-UCNPs (Figure 2d) in comparison with the oleylamine-coated OM-UCNPs (Figure S3). The results mentioned above indicate the successful assembly of the complex N719 on the surface of the as-prepared N719-UCNPs. Moreover, the ratio of Ru/RE (Y,Yb) was measured to be approximately 1.04%, indicating that the amount of the complex N719 on the sample N719-UCNPs was approximately 6.2 wt %.

The amount of the complex N719 on the surface of the N719-UCNPs was also determined by absorption spectroscopy. As shown in Figure S4 (Supporting Information), the absorbance at 541 nm corresponds

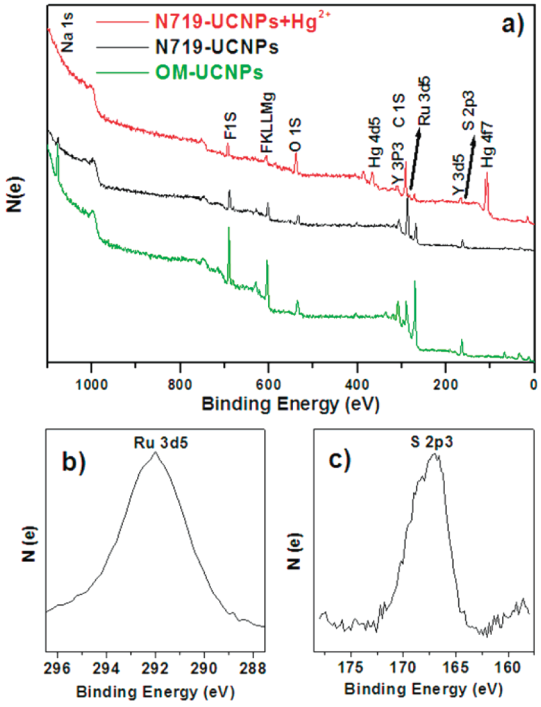

Figure 3. (a) XPS of OM-UCNPs (green line) and N719-UCNPs in the absence (black line) and presence (red line) of Hg^{2+}. (b,c) XPS of S element (b) and Ru element (c).

to 0.3 mg·mL^{-1} N719-UCNPs, meaning that the content of the complex N719 was 2.76 × 10^{-5} mol/L and that the amount of the complex N719 on sample N719-UCNPs was approximately 5.8 wt %. This result is similar to that obtained by EDXA (6.2 wt %). Considering the average diameter of 17 nm for N719-UCNPs (hexagonal phase), the average loading of the complex N719 could be calculated as ~670 units per N719-UCNP particle from the EDXA and absorption spectroscopy data (average loading amount 6% of N719).

To certify the efficiency of energy transfer of upconversion luminescence emission of UCNPs to absorption of the surface ligand N719, we investigated the quenching effect of upconversion luminescence emission of the simple mixing system of the complex N719 and PAA-coated UCNPs. In this control experiment, PAA can protect the surface of UCNPs and prevent the carboxyl group of the complex N719 to coordinate with rare-earth ion on the surface of UCNPs. As a result, the interaction of the complex N719 with PAA-coated UCNPs is negligent. As determined by luminescence spectroscopy, the upconversion luminescence quenching efficiency in 520–560 nm is about 5% for the mixing system of the complex N719 and PAA-coated UCNPs, whereas the upconversion luminescence quenching efficiency is about 51% for the N719-UCNPs, as shown in Figure S5. This fact demonstrated that the designed N719-UCNPs is the energy transfer nanosystem.

Hg^{2+}-Sensing Capabilities of N719-UCNPs. The sensing ability of ruthenium complex N719-modified upconversion

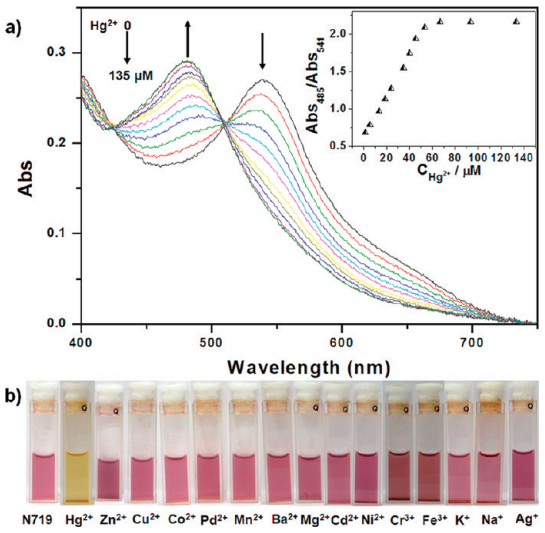

Figure 4. (a) Changes in absorption spectra of 0.3 mg·mL^{-1} N719-UCNPs (27.6 μM N719) in the aqueous solution upon gradual addition of Hg^{2+} ions (from 0 to 135 μM). Inset: the ratio (A_{485}/A_{541}) of absorbance at 485 and 541 nm. (b) Color change of the aqueous solution of N719-UCNPs in the presence of various representative metal ions.

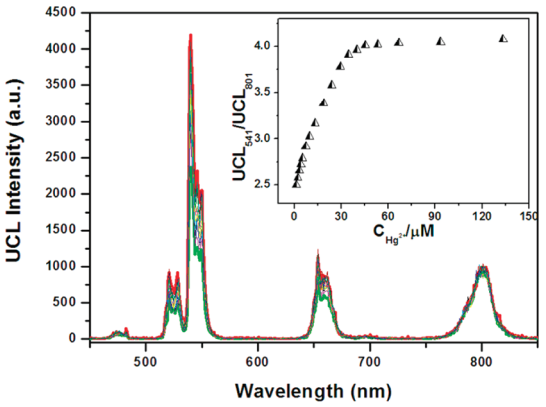

Figure 5. Upconversion luminescence spectra of 0.3 mg·mL^{-1} N719-UCNPs (27.6 μM N719) in the aqueous solution upon gradual addition of Hg^{2+} ions (from 0−135 μM). UCL_{541} means the upconversion luminescence between 538 to 544 nm (541 ± 3 nm), while UCL_{801} means upconversion luminescence at 801 ± 3 nm. Inset: the ratio (UCL_{541}/UCL_{801}) of upconversion luminescence intensities at 541 and 801 nm of N719-UCNPs as a function of Hg^{2+} concentration.

nanophosphor N719-UCNPs for Hg^{2+} was investigated by UV/vis absorption and upconversion luminescence emission spectroscopies. In the absorption spectrum (Figure 4a), N719-UCNPs show a broad visible band with the maximum wavelength of 541 nm, which can be attributed to metal-to-ligand charge transfer transitions (MLCT) of ruthenium complex N719. When the solution of $HgCl_2$ was added, the absorption peak was gradually blue-shifted to 485 nm. This blue shift of approximately 55 nm corresponds to a color change of the solution from red to orange (Figure 4b), indicating a strong interaction between the complex N719 and Hg^{2+}. As shown in Figure 4a inset, no further variation was measured after 55 μM Hg^{2+} had been added to 0.3 mg·mL^{-1} N719-UCNPs (corresponding to the complex N719 of 2.76 × 10^{-5} mol/L), indicating that the saturable concentration of Hg^{2+} was 2 equiv per N719 on the surface of N719-UCNPs. These facts indicated that the sulfur atom of each NCS group of the UCNP's surface ligand N719 coordinated to one Hg^{2+} ion, which is in agreement with previous observations.[58]

Importantly, as shown in Figure 5, the addition of Hg^{2+} caused an increase in the upconversion luminescence intensity at 520−540 and 650 nm but no change in the upconversion luminescence emission at 801 nm. As discussed above, addition of Hg^{2+} leads to decreasing spectral overlap between the visible upconversion luminescence emission of UCNPs and absorption of adduct N719-Hg^{2+}, thereby, FRET from the visible upconversion luminescence of UCNPs to the absorption of N719-Hg^{2+} is reduced, corresponding to an increasing green upconversion luminescence (Scheme 1). Considering the independence of the NIR upconversion luminescence emission at 801 nm on Hg^{2+}, this emission could be used as an internal standard reference and the ratio (UCL_{541}/UCL_{801}) of upconversion luminescence intensities at 541 and 801 nm was chosen as the output signal. The variation of this upconversion luminescence ratio (UCL_{541}/UCL_{801}) *versus* addition of Hg^{2+} is shown in the inset of Figure 5. The detection limit for Hg^{2+} in aqueous solution utilizing ratiometric upconversion luminescence spectroscopy is approximately 1.95 ppb (Figure S5), which is 1/10 that of the complex N719 in sensing Hg^{2+}[59] and reaches the maximum permissible level of Hg^{2+} ions in drinking water (2 ppb) set by the United States Environmental Protection Agency (EPA).

Furthermore, the time course of the response of N719-UCNPs (0.3 mg·mL^{-1}) to Hg^{2+} was investigated. The significant color change of N719-UCNPs from brick-red to yellow was observed within 10 s (movie in Supporting Information) upon addition of 5 equiv of Hg^{2+}. In addition, the response of Hg^{2+}-treated N719-UCNP to KI was investigated. Upon adding KI to a mixture of N719-UCNPs and Hg^{2+}, the yellow color of the solution changes to brick-red (Figure 6, inset), indicating strong interaction between Hg^{2+} and I^-, and then dissociation of Hg^{2+} from the adduct N719-Hg^{2+}. At the same time, upon addition of Hg^{2+}, the green upconversion luminescence emission is recovered to the original state of N719-UCNPs, while the NIR upconversion luminescence emission at 801 nm remains unchanged (Figure 6). Moreover, the recovery process with the addition of KI is completed within several seconds. Therefore, this nanosystem N719-UCNPs is suitably predisposed for the detection of Hg^{2+}.

High selectivity is necessary for an excellent chemodosimeter. In the present work, the optical responses of N719-UCNPs were extended to other metal cations in aqueous solution. Figure 4b and Figure 7

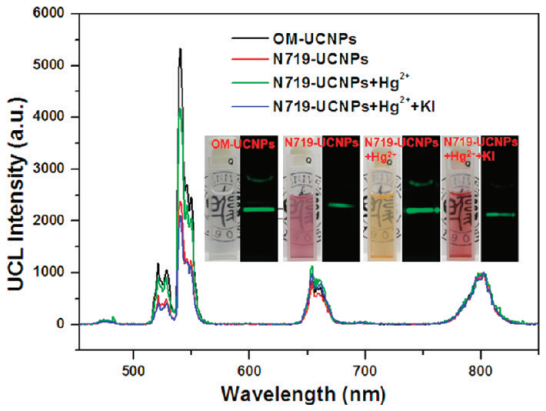

Figure 6. Normalized upconversion luminescence spectra of OM-UCNPs, N719-UCNPs in the absence and presence of Hg^{2+}, and Hg^{2+}-treated N719-UCNPs upon addition of KI. The inset shows bright-field and upconversion luminescence photos (with the band-pass filter of 540 ± 5 nm).

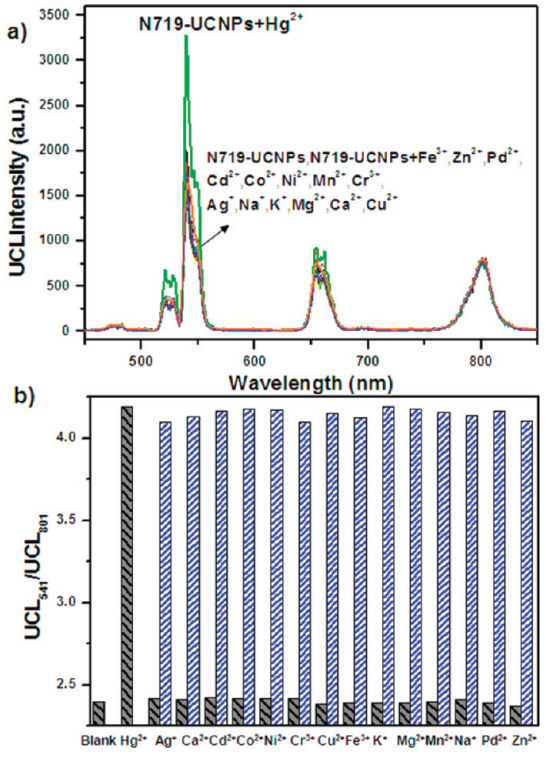

Figure 7. (a) Upconversion luminescence spectra of the aqueous solution of 0.3 mg·mL^{-1} N719-UCNPs (27.6 μM N719) in the presence of various representative metal ions. (b) Changes in UCL_{541}/UCL_{801} of 0.3 mg·mL^{-1} N719-UCNPs upon addition of 55.2 μM Hg^{2+}, 1 mM other metal cations (K^+, Ag^+, Mg^{2+}, Co^{2+}, Ni^{2+}, Mn^{2+}, Zn^{2+}, Cd^{2+}, Pd^{2+}, Cu^{2+}, Cr^{3+}, or Fe^{3+}), 27.6 mM Na^+, or 27.6 mM Ca^{2+}. Gray bars represent the upconversion luminescence response of N719-UCNPs to the cations of interest. Blue bars represent the subsequent addition of 55.2 μM Hg^{2+} to the above solution.

show the selectivity of the nanosystem N719-UCNPs as an optical sensor. As shown in Figure 4a, only the addition of Hg^{2+} led to drastic absorbance change of the N719-UCNPs, and no significant color changes were observed upon addition of other metal cations,

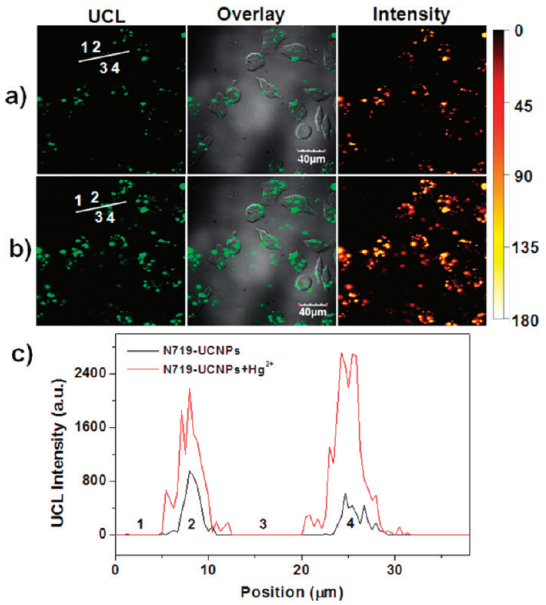

Figure 8. (a,b) Upconversion luminescence images and their overlays with bright-field images of HeLa cells incubated with 200 μg/mL N719-UCNPs for 3 h (a), and then incubated with Hg^{2+} for 15 min (b). (c) Upconversion luminescence intensity profile across the lines shown in panel a (black line) and b (red line) is shown in panel c (λ_{ex} = 980 nm; λ = 540 ± 20 nm).

such as Na^+, K^+, Ag^+, Ca^{2+}, Mg^{2+}, Co^{2+}, Ni^{2+}, Mn^{2+}, Zn^{2+}, Cd^{2+}, Pd^{2+}, Cu^{2+}, Cr^{3+}, and Fe^{3+}, indicating that only Hg^{2+} involved strong interaction with N719 moiety, resulting in the color change. Furthermore, as determined by UCL emission spectroscopy, only the addition of Hg^{2+} resulted in prominent changes in the ratio (UCL_{541}/UCL_{801}) of upconversion luminescence intensities at 541 and 801 nm, whereas the addition of large excesses of the other metal cations caused only slight changes, as shown in Figure 7a. Therefore, N719-UCNPs displayed high selectivity in upconversion luminescent sensing of Hg^{2+}. Moreover, competition experiments were carried out by adding Hg^{2+} to solutions of N719-UCNPs in the presence of other cations. As shown in Figure 7b, whether in the absence or presence of other cations, significant spectral changes were observed for N719-UCNPs upon addition of Hg^{2+}. The results indicate that the sensing of Hg^{2+} by N719-UCNPs is hardly affected by these commonly coexistent ions. Therefore, N719-UCNPs can act as a highly selective ratiometric upconversion luminescence probe for Hg^{2+}.

Sensing Hg^{2+} in Live Cells. To demonstrate the potential use of N719-UCNPs in bioimaging applications, we tested the cytotoxicity of N719-UCNPs toward HeLa cells, by the reduction activity of methyl thiazolyl tetrazolium (MTT) assay. As shown in Figure S7, upon incubation of 100−800 μg/mL N719-UCNPs for 24 and 48 h, no significant difference in the proliferation of the cells was observed. After incubation with N719-UCNPs for 24 h, the cellular viability was greater than 95%, and

the cell viability still remained >90% when the incubating time was prolonged to 48 h. The results of MTT assays attest that the N719-UCNPs have considerably low cytotoxicity.

Furthermore, a practical bioimaging application of N719-UCNPs for Hg^{2+} in biological samples was developed by laser scanning upconversion luminescence microscope (LSUCLM)[32] under CW excitation at 980 nm (Figure 8). The UCL emission at 540 ± 20 nm was used as the output signal of the collecting channel. The HeLa cells treated with only 200 μg/mL N719-UCNPs (18.4 μM) for 3 h at 37 °C showed a faint intracellular UCL signal, and the UCL intensity counts along the line in the UCL image, as shown in Figure 8a, were ~1000 (Figure 8c, black line). After further incubation with 40 μM Hg^{2+} ions in DMEM for 15 min at 37 °C, greatly enhanced intracellular UCL emission of the same cell was observed, and the UCL intensity counts, as shown in Figure 8b, were enhanced to be ~2500 (Figure 8c, red line). Moreover, the distribution of UCL intensity was analyzed with Kodak Molecular Imaging software. After incubating with 40 μM Hg^{2+} ions in DMEM for 15 min at 37 °C, the total UCL intensity integrate of the whole cell image was enhanced from 1.3×10^7 (for Figure 8a) to 4.5×10^7 (for Figure 8b), indicating that a significant variation in UCL intensity in the process of bioimaging of Hg^{2+}. Therefore, these results demonstrate that N719-UCNPs can be used to monitor Hg^{2+} in living cells using upconversion luminescence (UCL) emission microscopy technique.

CONCLUSION

In summary, we have demonstrated a highly selective water-soluble nanoprobe based on dye-assembled nanophosphors for upconversion luminescence sensing and bioimaging of mercury ions. The chromophoric ruthenium complex N719, as a Hg^{2+}-selective dye, was successfully assembled on the surface of UCNPs. This dye-assembled nanosystem of ratiometric upconversion luminescence can detect Hg^{2+} in aqueous solution with high selectivity, a rapid response time (<10 s), and with high sensitivity (detection limit of 1.95 ppb). Such detection limit of Hg^{2+} is only 1/10 of that of pure complex N719 in chromophoric sensing Hg^{2+} and is lower than the maximum level (2 ppb) of Hg^{2+} in drinking water set by the United States EPA. Importantly, the nanoprobe has been shown to be capable of monitoring changes in the distribution of Hg^{2+} in living cells by upconversion luminescence bioimaging. Our successful upconversion luminescence-based nanoprobe for sensing and bioimaging of Hg(II) provides a new design strategy of further novel probes for highly sensitive detection and bioimaging studies.

MATERIALS AND METHODS

Materials. All starting materials were obtained from commercial supplies and used as received. Rare-earth oxides Y_2O_3 (99.999%), Yb_2O_3 (99.999%), Er_2O_3 (99.999%), and Tm_2O_3 (99.999%), were purchased from Shanghai Yuelong New Materials Co. Ltd. Oleylamine (OM) (>90%) was purchased from Aldrich. N719 was purchased from Sheng Chemical Co., Ltd. Suzhou. Polyacrylic acid and trifluoroacetic acid were purchased from Sinopharm Chemical Reagent Co., Ltd. All other chemical reagents with analytical grade were used directly without further purification. Deionized water was used throughout. $RE(CF_3COO)_3$ was prepared with the literature method.[62]

Characterization. Powder X-ray diffraction (XRD) measurements were performed on a Bruker D4 diffractometer at a scanning rate of 1°/min in the 2θ range from 10 to 70° (Cu Kα radiation, λ = 1.54056 Å). The size and morphology of UCNPs were determined at a JEOL JEM-2010 low- to high-resolution transmission electron microscope (HR-TEM) operated at 200 kV. These as-prepared samples were dispersed in cyclohexane and dropped on the surface of a copper grid for TEM test. Fourier transform infrared (FT-IR) spectra were performed using an IRPRESTIGE-21 spectroscope (Shimadzu) with KBr pellets. The wavenumber range recorded was 400−4000 cm^{-1}.Thermogravimetric analysis (TGA) curves were recorded on a DTG-60H (Shimadzu) at a heating rate of 10 °C/min. The images of upconversion luminescence were obtained digitally on a Nikon multiple CCD camera. XPS experiments were carried out on a RBD upgraded PHI-5000C ESCA system (Perkin-Elmer) with Mg Kα radiation ($h\nu$ = 1253.6 eV) or Al Kα radiation ($h\nu$ = 1486.6 eV).

Synthesis of Oleylamine (OM)-Capped UCNPs (Abbreviated as OM-UCNPs). Oleylamine-capped UCNPs (OM-UCNPs) were prepared by a modified cothermolysis process.[60,61]

Assembly of Complex N719 on the Surface of UCNPs (Abbreviated as N719-UCNPs). Acetonitrile solutions of complex N719 (2 mmol in total) were added to the prepared UCNPs (50 mg) in a 10 mL round-bottomed flask. Initially, the nanoparticles were dispersed in the acetonitrile by ultrasonication, and then the mixture was stirred for 1 h at room temperature to obtain a homogeneous phase. Then, the mixture was centrifuged (15 455*g*, 8 min every time in 20 °C), and the collected solid was repeatedly washed with water and acetonitrile. The precipitate could be redispersed in deionized water or other polar solvents.

Synthesis of Polyacrylic Acid-Capped UCNPs (Abbreviated as PAA-UCNPs). PAA-UCNPs were prepared from oleylamine-capped UCNPs with poly(acrylic acid) , by a ligand exchange process.[63]

Average Molecular Weight. M_w(UCNP) of one UCNP on the nanoprobe N719-UCNP is calculated using the following equation.

$$M_{w(UCNP)} = \frac{\frac{4}{3}\pi R^3 \rho N_A}{1 - 6.0\%}$$

where R denotes the core radius (~8.5 nm), ρ is the density of crystal lattice of β-$NaYF_4$ nanoparticles (JCPDS card 16-0334, ρ = 4.309 g/cm^3), 6.0% stands for the content of N719 ligands determined by absorption spectroscopy. N_A is the Avogadro constant (6.02×10^{23}/mol). The average loading number (n) of complex N719 per nanoparticle N719-UCNP could be calculated as follows:

$$n = \frac{M_{w(UCNP)} \times 6.0\%}{(1 - 6.0\%) \times M_{w(Ru)}}$$

where M_w(UCNP) is average molecular weight of one UCNP on the nanoprobe N719-UCNP. M_w(Ru) is molecular weight of complex N719, and 6.0% stands for the content of N719 ligands, as determined by absorption spectroscopy.

Spectroscopic Measurements and Metal Cation Titration of N719-UCNPs. UV−vis spectra were recorded on a Shimadzu 3000 spectrophotometer. UCL spectra were measured on an Edinburgh LFS920 luminescence spectrometer with high stability of 980 nm pump laser source. Samples for absorption and

emission measurements were contained in 1 cm × 1 cm quartz cuvettes. Spectrophotometric titrations were performed on 0.3 mg/mL solutions of N719-UCNPs in H_2O. Typically, aliquots of fresh cations (Na^+, K^+, Ag^+, Ca^{2+}, Mg^{2+}, Co^{2+}, Ni^{2+}, Mn^{2+}, Zn^{2+}, Cd^{2+}, Pd^{2+}, Cu^{2+}, Cr^{3+}, and Fe^{3+}) were added, and the UV−vis absorption and fluorescent spectra of the samples were recorded.

Movie. Real-time change in color response of N719-UCNPs (20 μM) in aqueous solution upon addition of Hg^{2+} and then further addition of excessive KI. Then two drops Hg^{2+} aqueous solution (100 μM) was added, and the color was changed from brick-red to yellow within several seconds. After the addition of excessive KI, the color recovery to brick-red was completed within several second.

Cell Culture. The HeLa lines were provided by the Institute of Biochemistry and Cell Biology, SIBS, CAS (China). The HeLa cells were grown in DMEM (Dulbecco's modified Eagle's medium) supplemented with 10% FBS (fetal bovine serum), and culture was at 37 °C under 5% CO_2.

Cytotoxicity Assay. The *in vitro* cytotoxicity was measured using a standard methyl thiazolyl tetrazolium (MTT, Sigma-Aldrich) assay in HeLa cell lines. Briefly, cells growing in log phase were seeded into 96-well cell culture plate at 1×10^4/well. The UCNPs at concentrations of 100, 200, 400, and 800 μg/mL were added to the wells of the treatment group and 100 μL/well DMSO diluted in DMEM or RPMI 1640 at final concentration of 0.2% to the negative control group, respectively. The cells were incubated for 24 and 48 h at 37 °C under 5% CO_2. The combined MTT/PBS solution was added to each well of the 96-well assay plate and incubated for an additional 4 h. An enzyme-linked immunosorbent assay (ELISA) reader (infinite M200, Tecan, Austria) was used to measure the OD570 (absorbance value) of each well referenced at 690 nm. The following formula was used to calculate the viability of cell growth:

$$\text{viability}\ (\%) = (\text{mean of absorbance value of treatment group}\ /\text{mean of absorbance value of control}) \times 100$$

Luminescence Bioimaging. Cells (5×10^8/L) were plated on 14 mm glass coverslips and allowed to adhere for 24 h. The cells were washed with PBS and then incubated solely with 200 μg/mL N719-UCNPs in DMDEM for 3 h at 37 °C. Cell imaging was then carried out after washing the cells with PBS. Luminescence imaging was performed with an Olympus FluoView FV1000 confocal fluorescence microscope and a 60× oil immersion objective lens. Cells incubated with N719-UCNPs were excited at 980 nm with a CW laser, and the emission was collected at 540 ± 20 nm. Quantization by line plots was accomplished using the software package provided by Olympus instruments.

Acknowledgment. The authors thank National Science Foundation of China (20825101 and 91027004), MOST of China (2011AA03A407), Shanghai Sci. Tech. Comm. (11XD1400200 and 1052 nm03400), IRT0911, Shanghai Leading Academic Discipline Project (B108), and the CAS/SAFEA International Partnership Program for Creative Research Teams for financial support.

Supporting Information Available: (1) X-ray diffraction patterns (XRD) of the nanocrystal N719-UCNPs and standard β-phase $NaYF_4$. (2) FT-IR of OM-UCNPs, N719-UCNPs and free complex N719. (3) EDXA of OM-UCNPs. (4) The N719 concentration of N719-UCNPs was calculated using the detailed titration spectra. (5) Upconversion luminescence spectra of OM-UCNPs, N719-UCNPs, PAA-UCNPs in the absence and presence of Hg^{2+}. (6) The sensitivity test of N719-UCNPs toward Hg^{2+} using UCL emission technique. (7) *In vitro* cell viability of HeLa cells incubated with N719-UCNPs at different concentration for 24 and 48 h. This material is available free of charge *via* the Internet at http://pubs.acs.org.

REFERENCES AND NOTES

1. Cotton, F. A.; Willkinson, G.; Murillo, C. A.; Bochmann, M. In *Advanced Inorganic Chemistry*; Wiley: New York, 1999.
2. Kim, H. N.; Guo, Z. Q.; Zhu, W. H.; Yoon, J. Y.; Tian, H. Recent Progress on Polymer-Based Fluorescent and Colorimetric Chemosensors. *Chem. Soc. Rev.* **2011**, *40*, 79–93.
3. Nolan, E. M.; Lippard, S. J. Tools and Tactics for the Optical Detection of Mercuric Ion. *Chem. Rev.* **2008**, *108*, 3443–3480.
4. Zhao, Q.; Li, F. Y.; Huang, C. H. Phosphorescent Chemosensors Based on Heavy-Metal Complexes. *Chem. Soc. Rev.* **2010**, *39*, 3007–3030.
5. Quang, D. T.; Kim, J. S. Calixarene-Derived Fluorescent Probes. *Chem. Rev.* **2010**, *110*, 6280–6301.
6. Wu, D.; Descalzo, A. B.; Weik, F.; Emmerling, F.; Shen, Z.; You, X. Z.; Rurack, K. A Core-Modified Rubyrin with meso-Aryl Substituents and Phenanthrene-Fused Pyrrole Rings: A Highly Conjugated Near-Infrared Dye and Hg^{2+} Probe. *Angew. Chem., Int. Ed.* **2008**, *47*, 193–197.
7. Ros-Lis, J. V.; Marcos, M. D.; Martı́nez-Máñez, R.; Rurack, K.; Soto, J. A Regenerative Chemodosimeter Based on Metal-Induced Dye Formation for the Highly Selective and Sensitive Optical Determination of Hg^{2+} Ions. *Angew. Chem., Int. Ed.* **2005**, *44*, 4405–4407.
8. Liu, B.; Tian, H. A Selective Fluorescent Ratiometric Chemodosimeter for Mercury Ion. *Chem. Commun.* **2005**, 3156–3158.
9. Yang, Y. K.; Yook, K. J.; Tae, J. S. A Rhodamine-Based Fluorescent and Colorimetric Chemodosimeter for the Rapid Detection of Hg^{2+} Ions in Aqueous Media. *J. Am. Chem. Soc.* **2005**, *127*, 16760–16761.
10. Guo, Z. Q.; Zhu, W. H.; Shen, L. J.; Tian, H. A Fluorophore Capable of Crossword Puzzles and Logic Memory. *Angew. Chem., Int. Ed.* **2007**, *46*, 5549–5553.
11. Song, F. L.; Watanabe, S.; Floreancig, P. E.; Koide, K. Scalable and Concise Synthesis of Dichlorofluorescein Derivatives Displaying Tissue Permeation in Live Zebrafish Embryos. *J. Am. Chem. Soc.* **2008**, *130*, 16460–16461.
12. Ando, S.; Koide, K. Development and Applications of Fluorogenic Probes for Mercury(II) Based on Vinyl Ether Oxymercuration. *J. Am. Chem. Soc.* **2011**, *133*, 2556–2566.
13. Ko, S. K.; Yang, Y. K.; Tae, J. S.; Shin, I. *In Vivo* Monitoring of Mercury Ions Using a Rhodamine-Based Molecular Probe. *J. Am. Chem. Soc.* **2006**, *128*, 14150–14155.
14. Yang, H.; Zhou, Z. G.; Huang, K. W.; Yu, M. X.; Li, F. Y.; Yi, T.; Huang, C. H. Multisignaling Optical-Electrochemical Sensor for Hg^{2+} Based on a Rhodamine Derivative with a Ferrocene Unit. *Org. Lett.* **2007**, *9*, 4729–4732.
15. Wu, J. S.; Hwang, I. C.; Kim, K. S.; Kim, J. S. Rhodamine-Based Hg^{2+}-Selective Chemodosimeter in Aqueous Solution: Fluorescent OFF-ON. *Org. Lett.* **2007**, *9*, 907–910.
16. Zhang, X. L.; Xiao, Y.; Qian, X. H. A Ratiometric Fluorescent Probe Based on FRET for Imaging Hg^{2+} Ions in Living Cells. *Angew. Chem., Int. Ed.* **2008**, *47*, 8025–8029.
17. Choi, M. G.; Kim, Y. H.; Namgoong, J. E.; Chang, S.-K. Hg^{2+}-Selective Chromogenic and Fluorogenic Chemodosimeter Based on Thiocoumarins. *Chem. Commun.* **2009**, 3560–3562.
18. Yu, H. B.; Xiao, Y.; Guo, H. Y.; Qian, X. H. Convenient and Efficient FRET Platform Featuring a Rigid Biphenyl Spacer between Rhodamine and BODIPY: Transformation of `Turn-On' Sensors into Ratiometric Ones with Dual Emission. *Chem.—Eur. J.* **2011**, *17*, 3179–3191.
19. Lu, H.; Xue, Z. L.; Mack, J; Shen, Z.; You, X. Z.; Kobayashi, N. Specific Cu^{2+}-Induced J-Aggregation and Hg^{2+}-Induced Fluorescence Enhancement Based on BODIPY. *Chem. Commun.* **2010**, *46*, 3565–3567.
20. Guo, Z. Q.; Zhu, W. H.; Zhu, M. M.; Wu, X. M.; Tian, H. Hydrophilic Copolymer Bearing Dicyanomethylene-4*H*-Pyran Moiety as Fluorescent Film Sensor for Cu^{2+} and Pyrophosphate Anion. *Chem.—Eur. J.* **2010**, *16*, 14424–14432.
21. Auzel, F. Upconversion and Anti-Stokes Processes with f and d Ions in Solids. *Chem. Rev.* **2004**, *104*, 139–173.
22. Wang, F.; Liu, X. G. Recent Advances in the Chemistry of Lanthanide-Doped Upconversion Nanocrystals. *Chem. Soc. Rev.* **2009**, *38*, 976–989.
23. Wang, F.; Banerjee, D.; Liu, Y. S.; Chen, X. Y.; Liu, X. G. Upconversion Nanoparticles in Biological Labelling, Imaging, and Therapy. *Analyst* **2010**, *135*, 1839–1854.

24. Zhou, J.; Liu, Z.; Li, F. Y. Upconversion Nanophosphors for Small-Animal Imaging, *Chem. Soc. Rev.* **2011**, DOI: 10.1039/C1CS15187H.
25. Feng, W.; Sun, L. D.; Zhang, Y. W.; Yan, C. H. Synthesis and Assembly of Rare Earth Nanostructures Directed by the Principle of Coordination Chemistry in Solution-Based Process. *Coord. Chem. Rev.* **2010**, *254*, 1038–1053.
26. Haase, M.; Schäfer, H. Upconverting Nanoparticles. *Angew. Chem., Int. Ed.* **2011**, *50*, 5808–5829.
27. Fischer, L. H.; Harms, G. S.; Wolfbeis, O. S. Upconverting Nanoparticles for Nanoscale Thermometry. *Angew. Chem., Int. Ed.* **2011**, *50*, 4546–4551.
28. Achatz, D. E.; Meier, R. J.; Fischer, L. H.; Wolfbeis, O. S. Luminescent Sensing of Oxygen Using a Quenchable Probe and Upconverting Nanoparticles. *Angew. Chem., Int. Ed.* **2011**, *50*, 260–263.
29. Mader, H. S.; Wolfbeis, O. S. Optical Ammonia Sensor Based on Upconverting Luminescent Nanoparticles. *Anal. Chem.* **2010**, *82*, 5002–5004.
30. Wang, X.; Zhuang, J.; Peng, Q.; Li, Y. D. A General Strategy for Nanocrystal Synthesis. *Nature* **2005**, *437*, 121–124.
31. Chen, Z. G.; Chen, H. L.; Hu, H.; Yu, M. X.; Li, F. Y.; Zhang, Q.; Zhou, Z. G.; Yi, T.; Huang, C. H. Versatile Synthesis Strategy for Carboxylic Acid-Functionalized Upconverting Nanophosphors as Biological Labels. *J. Am. Chem. Soc.* **2008**, *130*, 3023–3029.
32. Yu, M. X.; Li, F. Y.; Chen, Z. G.; Hu, H.; Zhan, C.; Yang, H.; Huang, C. H. Laser Scanning Up-Conversion Luminescence Microscopy for Imaging Cells Labeled with Rare-Earth Nanophosphors. *Anal. Chem.* **2009**, *81*, 930–935.
33. Park, Y.; Kim, J. H.; Lee, K. T.; Jeon, K. S.; Na, H. B.; Yu, J. H.; Kim, H. M.; Lee, N.; Choi, S. H.; Aik, S. B.; *et al.* Nonblinking and Nonbleaching Upconverting Nanoparticles as an Optical Imaging Nanoprobe and T1 Magnetic Resonance Imaging Contrast Agent. *Adv. Mater.* **2009**, *21*, 4467–4471.
34. Kumar, M.; Nyk, R.; Ohulchanskyy, T. Y.; Flask, C. A.; Prasad, P. N. Combined Optical and MR Bioimaging Using Rare Earth Ion Doped $NaYF_4$ Nanocrystals. *Adv. Funct. Mater.* **2009**, *19*, 853–859.
35. Nyk, M.; Kumar, R.; Ohulchanskyy, T. Y.; Bergey, E. J.; Prasad, P. N. High Contrast *In Vitro* and *In Vivo* Photoluminescence Bioimaging Using Near Infrared to Near Infrared Up-Conversion in Tm^{3+} and Yb^{3+} Doped Fluoride Nanophosphors. *Nano Lett.* **2008**, *8*, 3834–3838.
36. Xiong, L. Q.; Chen, Z. G.; Tian, Q. W.; Cao, T. Y.; Xu, C. J.; Li, F. Y. High Contrast Upconversion Luminescence Targeted Imaging *in Vivo* Using Peptide-Labeled Nanophosphors. *Anal. Chem.* **2009**, *81*, 8687–8694.
37. Idris, N. M.; Li, Z.; Ye, L.; Sim, E. K. W.; Mahendran, R.; Ho, P. C. L.; Zhang, Y. Tracking Transplanted Cells in Live Animal Using Upconversion Fluorescent Nanoparticles. *Biomaterials* **2009**, *30*, 5104–5113.
38. Wang, C.; Chen, L.; Liu, Z. Drug Delivery with Upconversion Nanoparticles for Multi-functional Targeted Cancer Cell Imaging and Therapy. *Biomaterials* **2010**, *32*, 1110–1120.
39. Zhou, J.; Sun, Y.; Du, X.; Xiong, L. Q.; Hu, H.; Li, F. Y. Dual-Modality *In Vivo* Imaging Using Rare-Earth Nanocrystals with Near-Infrared to Near-Infrared (NIR-to-NIR) Upconversion Luminescence and Magnetic Resonance Properties. *Biomaterials* **2010**, *31*, 3287–3295.
40. Cao, T. Y.; Yang, Y.; Gao, Y.; Zhou, J.; Li, Z. Q.; Li, F. Y. High-Quality Water-Soluble and Surface-Functionalized Upconversion Nanocrystals as Luminescent Probes for Bioimaging. *Biomaterials* **2011**, *32*, 2959–2968.
41. Chen, X. Y.; Tu, D. T.; Liu, L. Q.; Ju, Q.; Liu, Y. S.; Zhu, H. M.; Li, R. F. Time-Resolved FRET Biosensor Based on Amine-Functionalized Lanthanide-Doped $NaYF_4$ Nanocrystals. *Angew. Chem., Int. Ed.* **2011**, *50*, 6306–6310.
42. Wang, G. F.; Peng, Q.; Li, Y. D. Upconversion Luminescence of Monodisperse CaF_2:Yb^{3+}/Er^{3+} Nanocrystals. *J. Am. Chem. Soc.* **2009**, *131*, 14200–14201.
43. Gai, S. L.; Yang, P. P.; Li, C. X.; Wang, W. X.; Dai, Y. L.; Niu, N.; Lin, J. Synthesis of Magnetic, Up-Conversion Luminescent, and Mesoporous Core–Shell-Structured Nanocomposites as Drug Carriers. *Adv. Funct. Mater.* **2010**, *20*, 1166–1172.
44. Li, Z. Q.; Zhang, Y. Monodisperse Silica-Coated Polyvinylpyrrolidone/$NaYF_4$ Nanocrystals with Multicolor Upconversion Fluorescence Emission. *Angew. Chem., Int. Ed.* **2006**, *45*, 7732–7735.
45. Boyer, J. C.; Carling, C. J.; Gates, B. D.; Branda, N. R. Two-Way Photoswitching Using One Type of Near-Infrared Light, Upconverting Nanoparticles, and Changing Only the Light Intensity. *J. Am. Chem. Soc.* **2011**, *132*, 15766–15772.
46. Wang, F.; Han, Y.; Lim, C. S.; Lu, Y.; Wang, J.; Xu, J.; Chen, H.; Zhang, C.; Hong, M.; Liu, X. G. Simultaneous Phase and Size Control of Upconversion Nanocrystals through Lanthanide Doping. *Nature* **2010**, *463*, 1061–1065.
47. Wang, F.; Wang, J.; Liu, X. G. Direct Evidence of a Surface Quenching Effection Size-Dependent Luminescence of Upconversion Nanoparticles. *Angew. Chem., Int. Ed.* **2010**, *49*, 7456–7460.
48. Liu, Y. S.; Tu, D. T.; Zhu, H. M.; Li, R. F.; Luo, W. Q.; Chen, X. Y. A Strategy To Achieve Efficient Dual-Mode Luminescence of Eu^{3+} in Lanthanides Doped Multifunctional $NaGdF_4$ Nanocrystals. *Adv. Mater.* **2010**, *22*, 3266–3271.
49. Mai, H.; Zhang, Y.; Si, R.; Yan, Z.; Sun, L. D.; You, L.; Yan, C. H. High-Quality Sodium Rare-Earth Fluoride Nanocrystals: Controlled Synthesis and Optical Properties. *J. Am. Chem. Soc.* **2006**, *128*, 6426–6436.
50. Schäfer, H.; Ptacek, P.; Zerzouf, O.; Haase, M. Synthesis and Optical Properties of KYF_4/Yb, Er Nanocrystals, and Their Surface Modification with Undoped KYF_4. *Adv. Funct. Mater.* **2008**, *18*, 2913–2918.
51. Vetrone, F.; Naccache, R.; Mahalingam, V.; Morgan, C. G.; Capobianco, J. A. The Active-Core/Active-Shell Approach: A Strategy To Enhance the Upconversion Luminescence in Lanthanide-Doped Nanoparticles. *Adv. Funct. Mater.* **2009**, *19*, 2924–2929.
52. Boyer, J. C.; Vetrone, F.; Cuccia, L. A.; Capobianco, J. A. Synthesis of Colloidal Upconverting $NaYF_4$ Nanocrystals Doped with Er^{3+}, Yb^{3+} and Tm^{3+}, Yb^{3+} via Thermal Decomposition of Lanthanide Trifluoroacetate Precursors. *J. Am. Chem. Soc.* **2006**, *128*, 7444–7445.
53. Abel, K. A.; Boyer, J. C.; van Veggel, F. C. J. M. Hard Proof of the $NaYF_4$/$NaGdF_4$ Nanocrystal Core/Shell Structure. *J. Am. Chem. Soc.* **2009**, *131*, 14644–14645.
54. Sivakumar, S.; van Veggel, F. C. J. M.; May, P. S. Near-Infrared (NIR) to Red and Green Up-Conversion Emission from Silica Sol–Gel Thin Films Made with $La_{0.45}Yb_{0.50}Er_{0.05}F_3$ Nanoparticles, Hetero-Looping-Enhanced Energy Transfer (Hetero-LEET): A New Up-Conversion Process. *J. Am. Chem. Soc.* **2007**, *129*, 620–625.
55. Cheng, L.; Yang, K.; Shao, M. W.; Lee, S. T.; Liu, Z. Multicolor *In Vivo* Imaging of Upconversion Nanoparticles with Emissions Tuned by Luminescence Resonance Energy Transfer. *J. Phys. Chem. C* **2011**, *115*, 2686–2692.
56. Wang, C.; Tao, H. Q.; Cheng, L.; Liu, Z. Near-Infrared Light Induced *In Vivo* Photodynamic Therapy of Cancer Based on Upconversion Nanoparticles. *Biomaterials* **2011**, *32*, 6145–6154.
57. Palomares, E.; Vilar, R.; Durrant, J. R. Heterogeneous Colorimetric Sensor for Mercuric Salts. *Chem. Commun.* **2004**, 362–363.
58. Coronado, E.; Galán-Mascrós, J. R.; Martí-Gastaldo, C.; Palomares, E.; Durrant, J. R.; Vilar, R.; Gratzel, M.; Nazeeruddin, M. K. Reversible Colorimetric Probes for Mercury Sensing. *J. Am. Chem. Soc.* **2005**, *127*, 12351–12356.
59. Nazeeruddin, M. K.; Censo, D. D.; Humphry-Baker, R.; Grätzel, M. Highly Selective and Reversible Optical, Colorimetric, and Electrochemical Detection of Mercury(II) by Amphiphilic Ruthenium Complexes Anchored onto Mesoporous Oxide Films. *Adv. Funct. Mater.* **2006**, *16*, 189–194.
60. Yi, G. S.; Chow, G. M. Synthesis of Hexagonal-Phase $NaYF_4$: Yb,Er and $NaYF_4$: Yb,Tm Nanocrystals with Efficient Up-Conversion Fluorescence. *Adv. Funct. Mater.* **2006**, *16*, 2324–2329.
61. Liu, Q.; Sun, Y.; Li, C. G.; Zhou, J.; Li, C. Y.; Yang, T. S.; Zhang, X. Z.; Yi, T.; Wu, D. M.; Li, F. Y. ^{18}F-Labeled Magnetic-Upconversion Nanophosphors *via* Rare-Earth Cation-Assisted Ligand Assembly. *ACS Nano* **2011**, *5*, 3146–3157.

62. Roberts, J. E. Lanthanum and Neodymium Salts of Trifluoroacetic Acid. *J. Am. Chem. Soc.* **1961**, *83*, 1087–1088.
63. Naccache, R.; Vetrone, F.; Mahalingam, V.; Cuccia, L. A.; Capobianco, J. A. Controlled Synthesis and Water Dispersibility of Hexagonal Phase $NaGdF_4$:Ho^{3+}/Yb^{3+} Nanoparticles. *Chem. Mater.* **2009**, *21*, 717–723.